



## Article

# Dynamic Image Representation in a Spiking Neural Network Supplied by Astrocytes

Sergey V. Stasenko \*  and Victor B. Kazantsev 

Moscow Institute of Physics and Technology, 117303 Moscow, Russia

\* Correspondence: stasenko@neuro.nnov.ru

**Abstract:** The mathematical model of the spiking neural network (SNN) supplied by astrocytes is investigated. The astrocytes are a specific type of brain cells which are not electrically excitable but induce chemical modulations of neuronal firing. We analyze how the astrocytes influence images encoded in the form of the dynamic spiking pattern of the SNN. Serving at a much slower time scale, the astrocytic network interacting with the spiking neurons can remarkably enhance the image representation quality. The spiking dynamics are affected by noise distorting the information image. We demonstrate that the activation of astrocytes can significantly suppress noise influence, improving the dynamic image representation by the SNN.

**Keywords:** spiking neural network; neuron–glial interactions; astrocyte

**MSC:** 37M05; 92-10



**Citation:** Stasenko, S.V.; Kazantsev, V.B. Dynamic Image Representation in a Spiking Neural Network Supplied by Astrocytes. *Mathematics* **2023**, *11*, 561. <https://doi.org/10.3390/math11030561>

Academic Editor: Pedro A. Castillo Valdivieso

Received: 22 November 2022

Revised: 17 January 2023

Accepted: 18 January 2023

Published: 20 January 2023



**Copyright:** © 2023 by the authors. Licensee MDPI, Basel, Switzerland. This article is an open access article distributed under the terms and conditions of the Creative Commons Attribution (CC BY) license (<https://creativecommons.org/licenses/by/4.0/>).

## 1. Introduction

The construction of biologically relevant models of the brain information processing still remains one of the key tasks of modern mathematical neuroscience. In neurobiology, key mechanisms of information processing concern synaptic transmission between the brain network neurons. Synaptic plasticity, e.g., adaptive changes in the connection strengths, is believed to be the main instrument of implementation learning and memory in the neural networks. Following the neurobiological studies, many mathematical models are targeted at describing experimental results and, hence, imitating brain functions has been proposed. However, it still remains a challenge as to how at the network level brain circuits can generate such finely tuned and effective information representation and processing.

In the last two decades, neurobiological experiments have revealed that neurons and neural networks are not alone in the brain universe. It was found that glial cells, particularly astrocytes, known before as just “supporting” cells providing mostly metabolic functions, can also participate in information processing by means of chemical regulations of neuronal activity and synaptic transmission [1–4]. The inclusion of the third player, e.g., astrocytes, in the classical “presynapse–postsynapse” signal transmission scheme led to the concept of a tripartite synapse [2,3,5]. Astrocytes, through calcium-dependent release of neuroactive chemicals (for example, glutamate), affect the pre- and postsynaptic compartments of the synapse. When spikes are generated by a presynaptic neuron, a neurotransmitter (for example, glutamate) is released from the presynaptic terminal. By diffusion, part of the chemicals leave the synaptic cleft and bind to metabotropic glutamate receptors (mGluRs) on the astrocyte, which may be located near the presynaptic terminal. Activation of metabotropic glutamate receptors G-mediated leads to the formation of inositol-1,4,5-triphosphate (IP<sub>3</sub>). This process, after a cascade of molecular transformations inside the astrocyte, leads to the release of Ca<sup>2+</sup> into the cytoplasm. It induces the release of the neuroactive chemicals called gliotransmitters (for example, glutamate, adenosine triphosphate (ATP), D-serine, GABA) back to the extrasynaptic space. Next, they bind

to pre- or postsynaptic receptors, resulting finally in the modulation of the efficiency of synaptic transmission, completing the feedback loop [6].

Many mathematical models were then proposed to explore the functional role of astrocytes in neuronal dynamics. They include the model of the “dressed neuron,” which describes the astrocyte-mediated changes in neural excitability [7,8], the model of the astrocyte serving as a frequency selective “gate keeper” [9], the model of the astrocyte regulating presynaptic functions [10] and many others. In particular, it was demonstrated that gliotransmitters can effectively control presynaptic facilitation and depression. The model of the tripartite synapse was recently employed to demonstrate the functions of astrocytes in the coordination of neural network signaling, in particular, spike-timing-dependent plasticity and learning [11–13], as a mechanism responsible for the generation of neural synchrony [14,15]. In models of astrocytic networks, communication between astrocytes has been described as  $\text{Ca}^{2+}$  wave propagation and synchronization of  $\text{Ca}^{2+}$  waves [16–21]. However, due to a variety of potential actions that may be specific for brain regions and neuronal sub types, the functional roles of astrocytes in network dynamics are still a subject of debate.

The role of astrocytes as collaborators of spiking neural networks (SNNs) in implementing learning and memory functions has been intensively discussed in recent computational models [22–24]. Specifically, it was demonstrated that the astrocytes serving at much slower time scale can help SNNs to distinguish highly overlapping images. Here, we present another SNN model accompanied by the astrocytes that can significantly enhance the recognition of information images encoded in the form of dynamical spiking patterns stored by the SNN.

## 2. The Model

### 2.1. Mathematical Model of a Single Neuron

The individual neuron of the SNN is described by the Hodgkin–Huxley model [25,26] which determined that the squid axon carries three major currents: voltage-gated persistent  $\text{K}^+$  current,  $I_K$ , with four activation gates (resulting in the term  $n^4$  in the equation below, where  $n$  is the activation variable for  $\text{K}^+$ ), voltage-gated transient  $\text{Na}^+$  current,  $I_{Na}$ , with three activation gates and one inactivation gate (term  $m^3h$  below), and Ohmic leak current,  $I_L$ , which is carried mostly by  $\text{Cl}^-$  ions. The complete set (Equation (1)) of space-clamped Hodgkin–Huxley equations is

$$\begin{aligned} C\dot{V} &= I_{inj} - \overbrace{\bar{g}_{Na}m^3h(V - V_{Na})}^{I_{Na}} - \overbrace{\bar{g}_Kn^4(V - V_K)}^{I_K} - \overbrace{\bar{g}_L(V - V_L)}^{I_L} \\ \dot{n} &= \alpha_n(V)(1 - n) - \beta_n(V)n \\ \dot{m} &= \alpha_m(V)(1 - m) - \beta_m(V)m \\ \dot{h} &= \alpha_h(V)(1 - h) - \beta_h(V)h, \end{aligned} \quad (1)$$

where

$$\begin{aligned} I_{inj} &= I_{stim} + I_{noise} + I_{syn} \\ \alpha_n(V) &= \frac{0.01(V + 55)}{1 - \exp[-(V + 55)/10]} \\ \beta_n(V) &= 1.125 \exp[-(V + 65)/80] \\ \alpha_m(V) &= \frac{0.1(V + 40)}{1 - \exp[-(V + 40)/10]} \\ \beta_m(V) &= 4 \exp[-(V + 65)/18] \\ \alpha_h(V) &= 0.07 \exp[-(V + 65)/20] \\ \beta_h(V) &= \frac{1}{1 + \exp[-(V + 35)/10]} \end{aligned} \quad (2)$$

Shifted Nernst equilibrium potentials for  $I_{Na}$ ,  $I_K$  and  $I_L$  are  $V_{Na} = 50$  mV,  $V_K = -77$  mV and  $V_L = -54.4$  mV, respectively. Typical values of maximal conductances for  $I_{Na}$ ,  $I_K$  and  $I_L$  are  $\bar{g}_{Na} = 36$  mS/cm<sup>2</sup>,  $\bar{g}_K = 120$  mS/cm<sup>2</sup> and  $\bar{g}_L = 0.3$  mS/cm<sup>2</sup>, respectively. The functions  $\alpha(V)$  and  $\beta(V)$  describe the transition rates between open and closed states of the channels.  $C = 1$  F/cm<sup>2</sup> is the membrane capacitance, and  $I_{inj}$  (Equation (2)) is the applied current, which consists of three parts:  $I_{stim}$ ,  $I_{noise}$  and  $I_{syn}$ .

## 2.2. Applied Currents

Images applied to the SNN were encoded as matrices  $M$  of size  $n \times k$  and values from 0 to 1 for each pixel, where 0 is the absence of color, and  $n$  and  $k$  are the corresponding image sizes (length and width). Next, the matrix  $M$  was transformed into an  $l \times 1$  vector  $S$ , where  $l = n \times k$  and corresponds to the neuron index in the neural network. Thus, the stimulation current,  $I_{stim}$ , will be written in the following form:

$$I_{stim} = S \times A_S, \quad (3)$$

where  $A_S$  is the amplitude of stimulus taken here for illustration with value 5.3 nA.

The synaptic current,  $I_{syn}$ , is modeled using the conductance-based approach as the following form:

$$I_{syn} = g_j(V_j - E_j), \quad (4)$$

where

$$\dot{g}_j = \frac{-g_j}{\tau_j} \quad (5)$$

In our model, index  $j$  is used for excitatory (exc) and inhibitory (inh) synapses. Reversal potentials for synaptic currents are equal 0 mV and  $-80$  mV for excitatory and inhibitory synapses, respectively.  $\tau_j$  is the time relaxation which equaled 5 ms and 10 ms for excitatory and inhibitory synapses, respectively. Excitatory (inhibitory) synapses will increase the excitatory (inhibitory) conductance in the postsynaptic cell whenever a presynaptic action potential arrives at

$$g_j \leftarrow g_j + w_j, \quad (6)$$

where  $w_j$  is the synaptic weight equaling 3 nS and 77 nS for excitatory and inhibitory synapses, respectively.

Besides the synaptic input, each neuron receives a noisy thalamic input ( $I_{noise}$ ). The noisy thalamic input is applied to each neuron and generated in a random way from a standard normal distribution (i.e., normally distributed numbers with a mean of 0 and a standard deviation of 1).

Each spike in the neuron model induces the release of a neurotransmitter. To describe the neuron to astrocyte cross-talk, here, we only focus on the excitatory neurons releasing glutamate. Following earlier experimental and modeling studies, we assume that the glutamate–mediate exchange was the key mechanism to induce coherent neuronal excitations [27,28]. The role of GABAergic neurons in our network is to support the excitation and inhibition balance, avoiding hyperexcitation states.

For simplicity, we take a phenomenological model of released glutamate dynamics. In the mean field approximation, the average concentration of synaptic glutamate concentration for each excitatory synapse,  $X_e$ , was described by the following equations:

$$X_e(t) = \begin{cases} X_e(t_s) \exp(-t/\tau_X), & \text{if } t_s < t < t_{s+1}, \\ X_e(t_s - 0) + 1, & \text{if } t = t_s, \end{cases} \quad (7)$$

where  $e = 1, 2, 3, \dots$  is the index of excitatory presynaptic neurons,  $s = 1, 2, 3, \dots$  is the index of the presynaptic spikes, and  $\tau_X$  is the time relaxation equal to 80 ms. After the spike is generated on the presynaptic neuron, the neurotransmitter is released.

### 2.3. Tripartite Synapses

To describe the dynamics of a tripartite synapse, we used the mean-field approach to describe changes in the concentration of neuroactive substances (neurotransmitter and gliotransmitter), proposed in the work [29]. In the proposed model, the filtering of the external noise signal applied to neurons is carried out due to synaptic depression, which consists of a decrease in the probability of neurotransmitter release, which in turn leads to a decrease in the strength of the connection between neurons (work [30]). Part of the synaptic glutamate can bind to metabotropic glutamate receptors of the astrocyte processes. Next, after a cascade of molecular transformations mediated by the elevation of intracellular calcium, the astrocyte releases gliotransmitter back to the extracellular space. For our purpose, in the mathematical model, we dropped the detailed description of these transformations, defining only input–output functional relation between the neurotransmitter and gliotransmitter concentrations in the following form [29,31]:

$$dY_e = -Y_e/\tau_{Y_e} + \frac{\beta_Y}{1 + \exp(-X_e + X_{thr})} \quad (8)$$

where  $e = 1, 2, 3, \dots$  is the index of the excitatory neuron,  $Y_e$  is the gliotransmitter concentration in the neighborhood of the corresponding excitatory synapse, and  $\tau_{Y_e}$  is the clearance rate equal 120 ms. The second term in Equation (8) describes the gliotransmitter production ( $\beta_Y = 1$ ) when the mean field concentration of the gliotransmitter exceeds some threshold,  $X_{thr}$ , equal to 1. Figure 1 illustrates the network construction and neuron to astrocyte crosstalk for excitatory glutamatergic synapses.

It follows from experimental facts that astrocytes can influence the probability of neurotransmitter release [32–34]. In turn, it results in modulation synaptic currents. We accounted astrocytic synaptic depression in the following form for glutamatergic synapses:

$$w_{ext} \leftarrow w_{ext} \left( 1 - \frac{\gamma_Y}{(1 + \exp(-Y + Y_{thr}))} \right) \quad (9)$$

where  $w_{ext}$  is the weight for glutamatergic synapses between neurons, and  $\gamma_Y$  is the coefficient of astrocyte influence (in our case, synaptic depression) on synaptic connection.

### 2.4. Neural Network

A schematic representation of network with astrocytic modulation of probability release of neurotransmitter is presented in Figure 1a. After the generation of an action potential on the presynaptic neuron, the neurotransmitter is released from the presynaptic terminal. Its part can diffuse out of the cleft where it can bind to specific astrocyte receptors [35]. The activation of the astrocyte results in the generation of calcium transients in the form of short-term increase in the intra-cellular concentration of calcium. In turn, the calcium elevations lead to gliotransmitter (particularly glutamate) release. The released gliotransmitter, reaching the presynaptic terminal, leads to a change in the probability of neurotransmitter release, depressing the synaptic current.

The size  $N$  of the spiking neural network was chosen based on the size of the presented image, i.e.,  $N = n \times k$  in real time (resolution 1 ms). Motivated by the anatomy of a mammalian cortex, we chose the ratio of excitatory to inhibitory neurons to be 4 to 1. The probability of connection of excitatory neurons is 5%, and the probability of the connection of inhibitory neurons is 10%. Since the model uses a mean-field approach to describe changes in the main neuroactive substances (neurotransmitter and gliotransmitter), we do not separate the effect of a single astrocyte on a group of neurons or a group of neurons on a single astrocyte, but we introduce into the description of each synaptic contact

its own dynamics for the neuro- and gliotransmitters. In the case of our model, there is no need to balance the speed difference between neurons and astrocytes. Different time scales here serve as the mechanisms of image representation enhancement because the activation of astrocytes occurs as a cascade of biochemical reactions in response to integral neuronal activity [2,5]. For our purpose, we do not consider in the model inter-astrocyte connections formed in living networks by gap junctions. Such connections are of a diffusive type, resulting in a slow diffusion (relative to neuronal processes) of information in the network space that does not greatly affect the evaluated images. Thus, our model represents a compromise between the biophysically relevant description of the spiking neural networks and mean-field approximation of the astrocyte modulation dynamics.

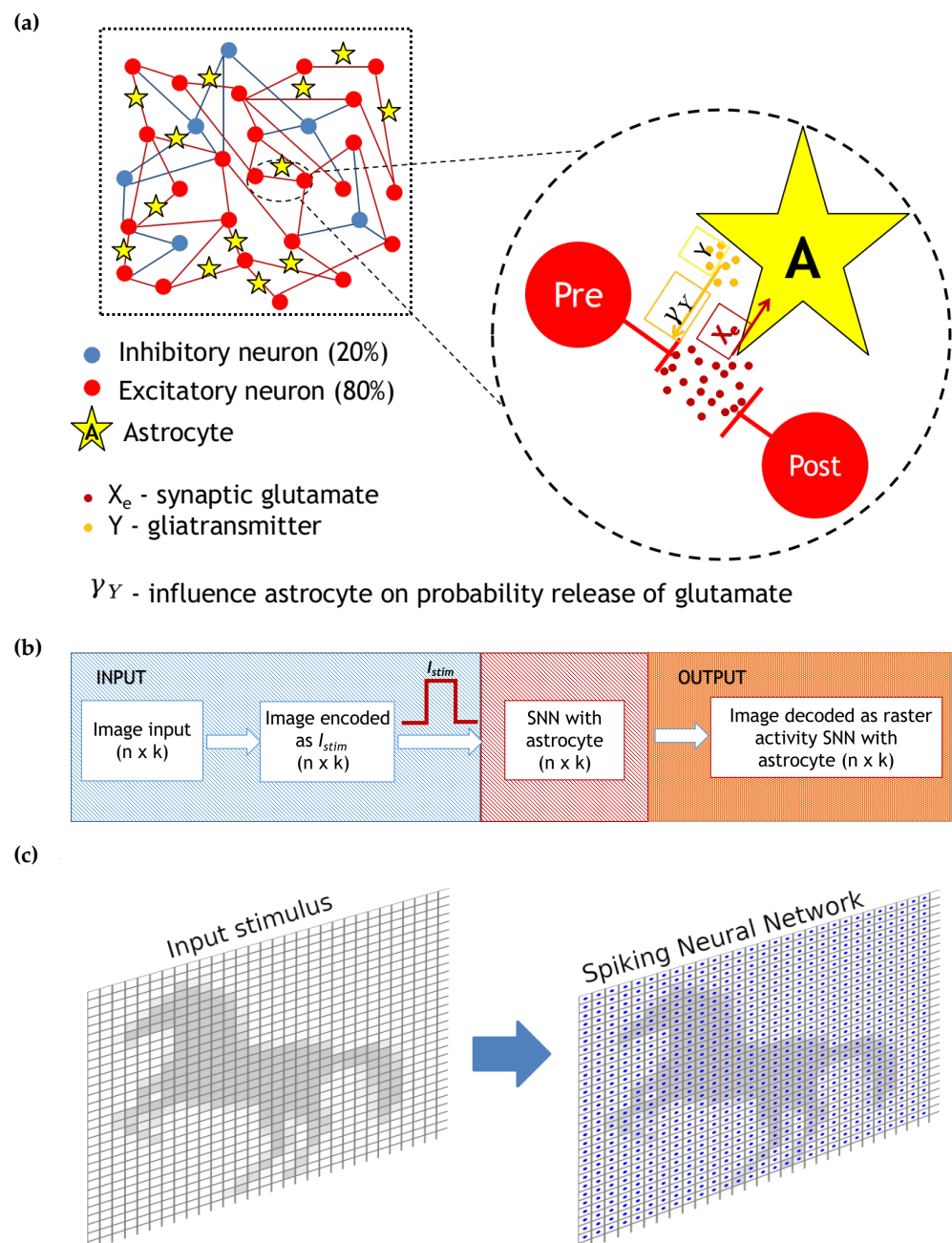


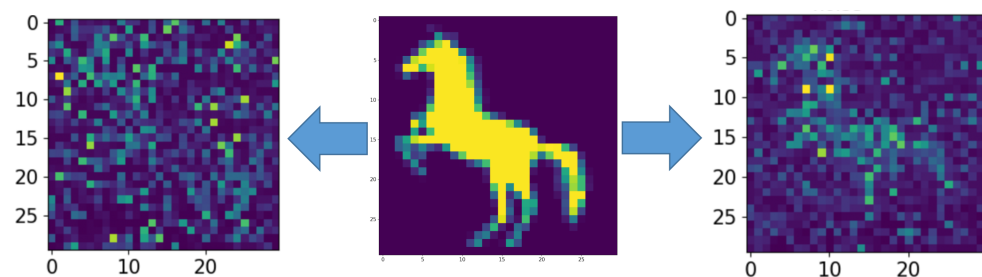
**Figure 1.** (a) Scheme of neuron–astrocyte network. (b) Scheme of encoded and decoded image input in spiking neural network with astrocyte regulation. (c) Schematic view of an input image load into the spiking neural network. Neurons (the blue dots) are arranged as two-dimensional lattice directly corresponding to image’s pixels.

### 2.5. Numerical Simulation Method

Numerical integration was performed using the Euler method (for additive stochastic differential equations using the Euler–Maruyama method) with a step of 0.01 ms. Numerical methods and data analysis were implemented in Python programming language [36] using the Numpy library for arrays, Pandas library for data processing and analysis, Brian2 [37] for model simulation and Matplotlib [38] and Seaborn libraries for data visualization and analysis.

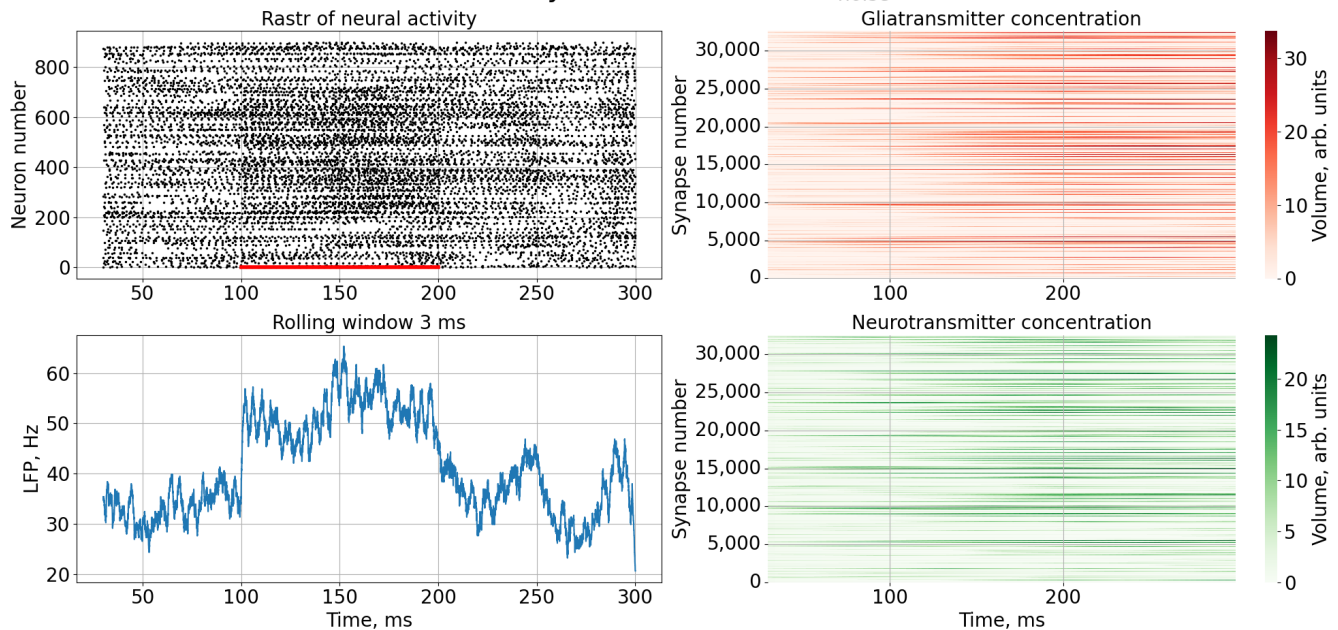
### 3. Results

Figure 1b illustrates the functional scheme of the model dynamics and the information flow. The model network was not initially structured somehow. It represented a fully connected graph with different connection probability (excitatory neurons 5%, inhibitory neurons 10%). When applying a stimulation patterns, we considered images of 30 by 30 pixels fed to a neural network of 900 neurons (the diagram is shown in Figure 1c). For illustration purposes, we artificially arranged our network in a two-dimensional lattice and associated each pixel of the image with a particular neuron location in this lattice. The input was formed by stimulation currents whose amplitudes and durations encoded the information image. The output was processed from values of neuron membrane potentials decoding time moments of spiking events. To demonstrate the effect of an astrocyte on the neural activity of a spiking neural network, the problem of representing an image by a neural network in the presence of noise was considered. For this purpose, an image in the form of a horse (in Figure 2, middle panel, was fed to the spiking neural network including tripartite synapses for 100 ms (Figures 3 and 4).

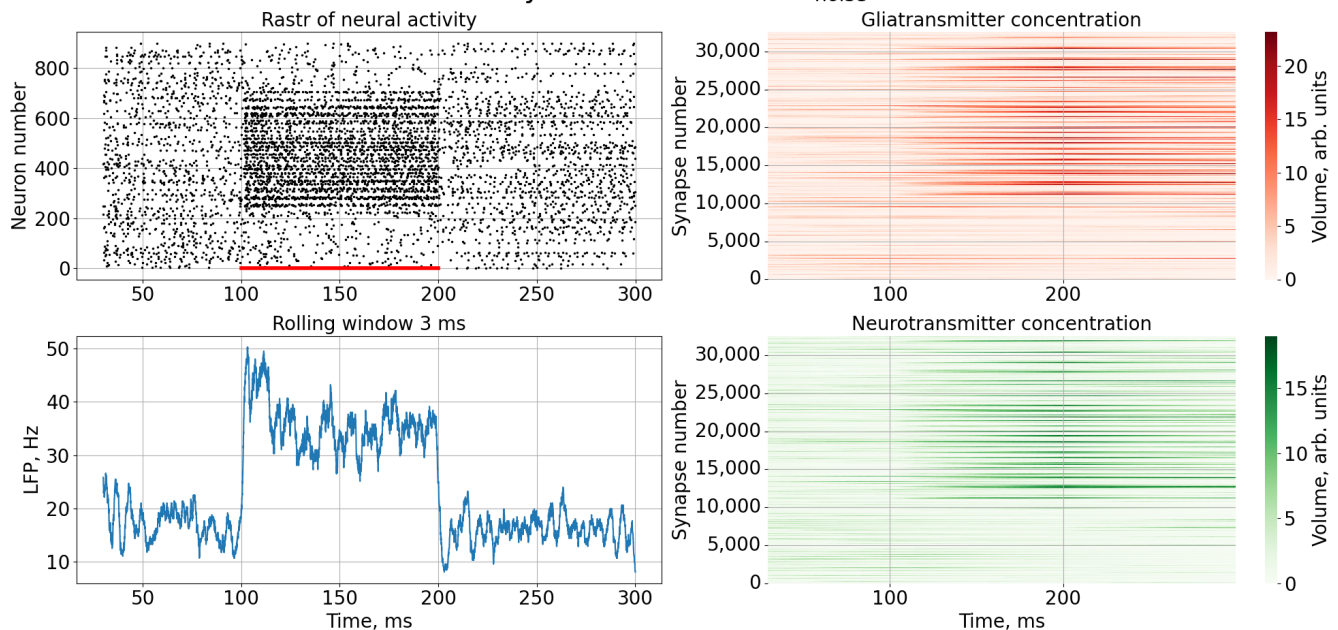


**Figure 2.** The middle picture is the supplied pattern (image of the horse), on the left, encoded by the spiking neural network without astrocyte modulation and noise amplitude  $A_{noise} = 6$ , and on the right, with astrocyte modulation and noise amplitude  $A_{noise} = 6$ .



No astrocyte modulation for  $A_{noise} = 6$ 

**Figure 3.** Time series of neural activity (upper left figure in the form of a raster diagram), the corresponding LFP signal with rolling window 3 ms (lower left figure) and time series of concentration gliotransmitters (upper right figure) and concentration neurotransmitters (lower right figure) in the case of an external noise signal with  $A_{noise} = 6$  without astrocytic modulation.

Astrocyte modulation for  $A_{noise} = 6$ 

**Figure 4.** Time series of neural activity (upper left figure in the form of a raster diagram), the corresponding LFP signal with rolling window 3 ms (lower left figure) and time series of concentration gliotransmitters (upper right figure) and concentration neurotransmitters (lower right figure) in the case of an external noise signal with  $A_{noise} = 6$  with astrocytic modulation.

A noise signal,  $I_{noise}$ , is applied to each neuron of the spiking neural network throughout the simulation. As can be replaced, as the amplitude,  $A_{noise}$ , of the noise signal increases without astrocytic modulation (Figure 5), blurring of the supplied image occurs. Activation

of the astrocyte (Figure 6) through the regulation of the neurotransmitter release probability leads to a balancing of excitation and inhibition in the network and thus stabilization of the image representation as the amplitude of the noise signal increases. Needless to say, the astrocytes depress the synaptic weights but do not significantly affect the overall performance of the spiking neural network. Note that noise current, stimulation current, and synaptic current contributed simultaneously to each spiking neuron activation. Being separated from the neuronal layer by construction, the astrocytes, in fact, serving as low-pass filters, reduced the noise component of total input current, thereby correcting the synaptic connections in a stimulus-dependent manner, hence improving the representation of the stimulus. In other words, the astrocyte action was stimulus-specific, which preserved the SNN performance in the presence of overall synaptic depression.

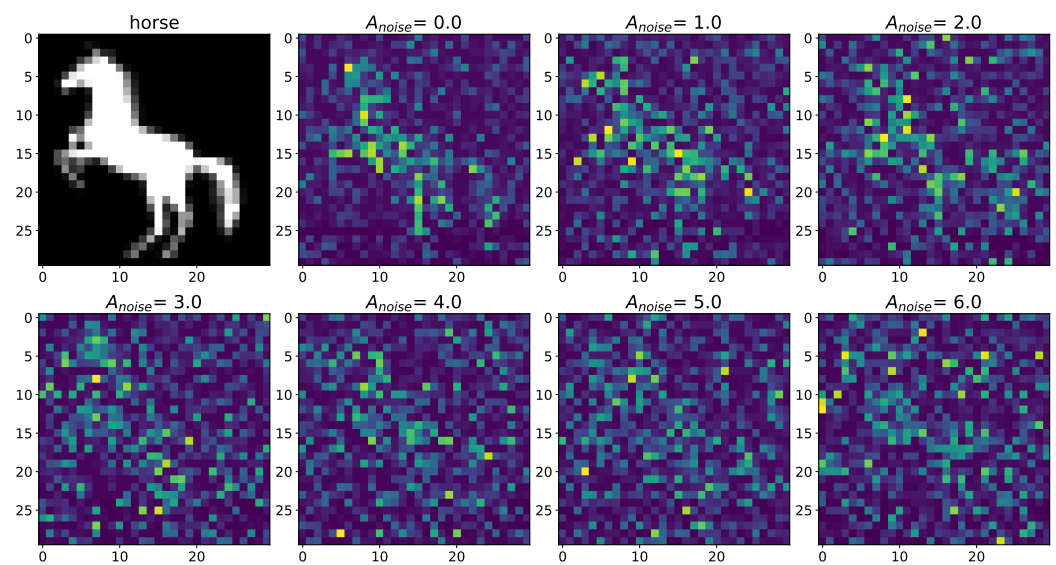


**Figure 5.** Changes in the spatial sweep of the spiking neural network during the representation of the supplied image from the Figure 2 when the amplitude,  $A_{noise}$ , of the noise current,  $I_{noise}$ , changes from 0 to 6 without modulation of neuronal activity by astrocytes.

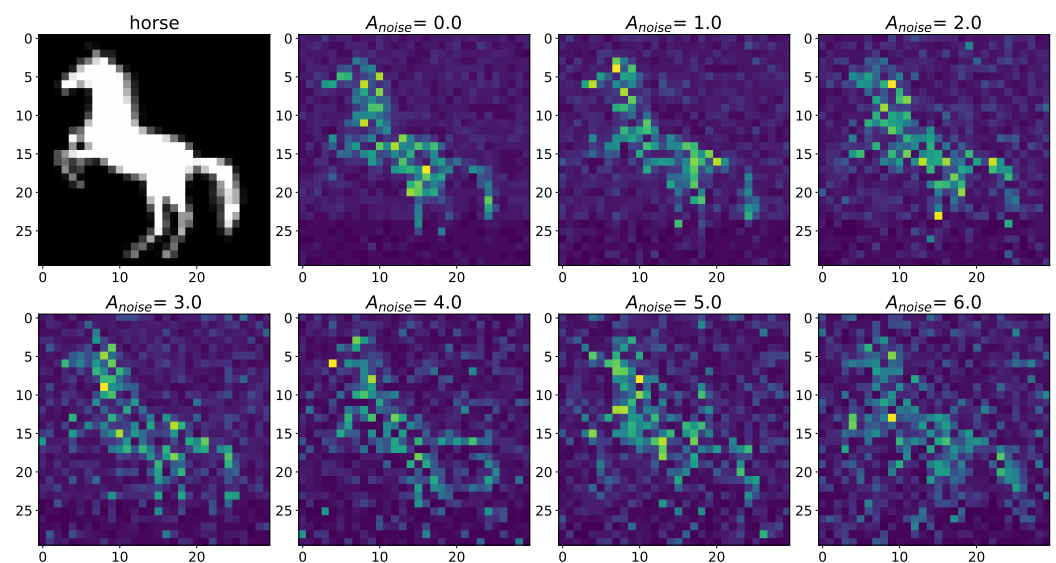


**Figure 6.** Changes in the spatial sweep of the spiking neural network during the representation of the supplied image from Figure 2 when the amplitude,  $A_{noise}$ , of the noise current,  $I_{noise}$ , changes from 0 to 6 with modulation of neuronal activity by astrocytes.



Next, we tested the model for different datasets. Additional results obtained using other input images (numbers from the database MNIST [39], categories from databases Fashion-MNIST [40] and SVHN [41]) are illustrated in Appendix A and in the Supplementary Materials. One can note that the model worked quite well for sufficiently contrasting images without color gradations (numbers from the database MNIST), but poorly with images that have color gradation (for example, grayscale) or fuzzy images (categories from databases Fashion-MNIST and SVHN). It is explained by the fact that the neural network itself is a coarse filter, where the neuron encodes a signal through a binary state: activated/inactivated. In addition, astrocytic dynamics form a second-level filter since the concentration of the gliotransmitter represents a slow variable in relation to the change in the membrane potential of the neuron, which is a fast variable.

This effect can be most clearly demonstrated by comparing rasters of neural activity (Figures 3 and 4) and the corresponding LFP signals (Figure 7) in the case of a high noise signal amplitude,  $A_{noise} = 6$ , in the presence and absence of astrocytic modulation. As can be seen, the astrocyte lowers the average activity of the neural network (gray area in Figure 7).

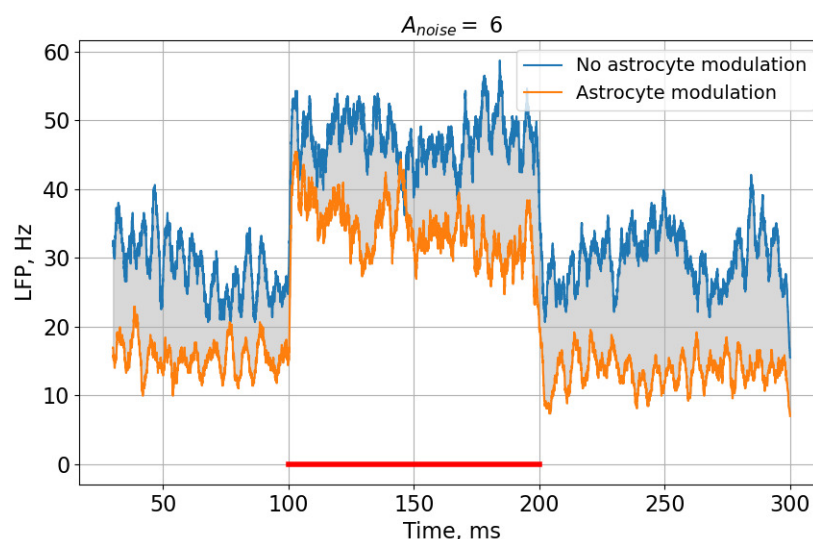


**Figure 7.** Comparison of the regulation of neuronal activity in the absence and presence of astrocytic modulation for a LFP signal with a noise current amplitude,  $A_{noise} = 6$ . The red line indicates the time of feeding the image to the neural network.

Figure 8 shows a comparison of raster diagrams of neural activity with the image supplied to the neural network over the entire considered range of change in the amplitude,  $A_{noise}$ , of the noise signal using the following quality metrics: MSE, RMSE, UQI, PSNR, SSIM, SCC, VIFP, PSNRB. It happened that the most appropriate metric for comparing our images was UQI because the UQI metric revealed differences from the point of view of “visual” comparison [42]. UQI is an image quality technique largely used to evaluate and assess the quality of images and is described in [43]. This metric was used for modeling any image distortion as a combination of three factors: correlation loss, brightness distortion, and contrast distortion. The value of the metric was in the range from 0 to 1, where 1 indicates that the images were completely identical and 0 that they were completely different. The higher value of the metric corresponded to the best similarities of the compared images. It demonstrated better results than the widely used distortion metric mean squared error. For the purpose of comparing images in the field of computer vision and machine learning, there are other metrics (in particular, MSE, RMSE, PSNR, SSIM, SCC, VIFP, and PSNRB) [42], which were also calculated for our compared images. The paper does not consider the metric of recognition accuracy, because here, we focus only on the problem of the input image representation of a spiking neural network. One can note that the different metrics considered demonstrated significant differences between cases with

and without astrocytic regulation. For example, for the UQI metrics, one can see that in the absence of astrocyte modulation (blue dots and curve in Figure 8), there was a linear decrease in the image similarity. When astrocytes were activated (red dots and curve in Figure 8), quite a significant drop in the similarity was observed in the range of noise signal amplitude values from 0 to 3.

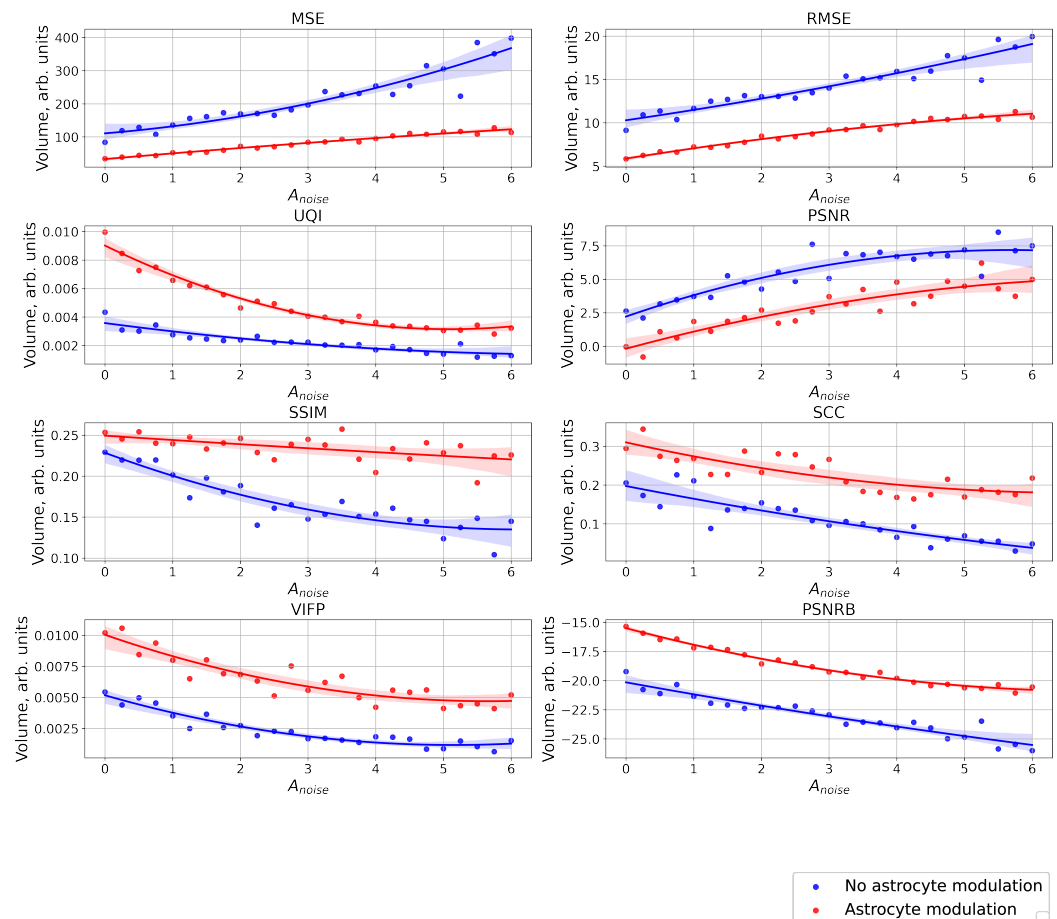


**Figure 8.** The case of using quality metrics—MSE, RMSE, UQI, PSNR, SSIM, SCC, VIFP, PSNRB—for comparing raster diagrams of neural activity from Figures 5 and 6 with an image (middle panel of Figure 2) fed to a spiking neural network with an increase in the amplitude,  $A_{noise}$ , of the noise signal from 0 to 6 supplied to the neurons of the neural network without astrocytic modulation (blue dots and curve) and with astrocytic modulation (red dots and curve).

#### 4. Conclusions

We developed a SNN model accompanied by astrocytes capable of implementing effective information encoding and its robust representation in the network with respect to noise perturbations. For illustration, we imposed an arbitrary binary image to the SNN that was kept therein in the form of *dynamic spiking pattern* encoded in the rate of spikes between different neurons. Obviously, in the purely deterministic case, it was recognized quite clearly. In practical situations, noise may significantly affect the quality of image representation. Activation of astrocytes made the network quite resistant to perturbations and significantly suppressed the effect of noise, preserving the shape of the original image. To evaluate such an astrocyte-mediated protection effect, we calculated changes of image quality characteristics following the quality metrics MSE, RMSE, UQI, PSNR, SSIM, SCC, VIFP, and PSNRB. It was demonstrated that the astrocytes were quite effective in improving the image quality recognition.

Thus, a key novel point of our model is the involvement of astrocytes in spiking neural network dynamic representation of information images. One of the advantages

of the model is that the astrocytes, being composed as separate layer, were able provide an additional way of controlling the synaptic connections in the spiking neural network independently on synaptic weight changes. However, the model faced problems when processing certain sets of images (numbers from the database MNIST, and categories from databases Fashion-MNIST and SVHN) with color gradation (for example, grayscale) or fuzzy images (categories from databases Fashion-MNIST and SVHN). This was primarily due to the fact that the neural network itself is a coarse filter, where the neuron encodes a signal through a binary state: activated/inactivated.

## 5. Discussion

As a point for discussion, we feel that astrocytes, besides their obvious functional role of low-pass filtering due to the slower time scale of the intrinsic process, also serve as an information processing *buffer* capable of storing dynamically basic features of the information pattern. Note that our results are consistent with recent studies of working memory proposed in the recent modeling paper [22]. We also note that the gate keeping function of astrocytes leads to the temporal depression of synaptic transmission in neighboring synapses as well as a noise reduction factor when local and relatively fast perturbations are filtered by the gliotransmitter dynamics.

Needless to say, the neuron–astrocyte–neuron connection values were not specifically trained. Nevertheless, the dynamic spiking pattern demonstrated effective representation of different desired images for a wide range of noise perturbations, including rather large noise amplitudes. In such a context, the astrocytes served as *non-specific information protectors* for neuronal signaling, employing spike-firing patterns. Needless to say, our model has no limits for processing larger and asymmetric pictures because the network (originally unstructured) can be structured artificially in any “stimulus-specific” manner. The only point is that the number of neurons should be equal to the number of pixels.

On the other hand, of course, the model represents a rather mathematical simplification of real brain circuits. However, at the level of local synaptic contacts, it employs basic principles of astrocytic modulation verified in many experimental works [2,5,6,35,44–47]. In recent experimental works, similar effects of local modulations by astrocytes on information processing and brain cognitive functions, such as memory and learning, were intensively discussed [48–51].

Note also that in the current model construction, we played mostly with the stimulus-specific excitation of SNN neurons that encoded information images. That is why, from a biological standpoint, we took the astrocyte-dependent modulation of excitatory synapses only. The inhibitory neurons served here a supporting role preserving excitation/inhibition balance. The use of the modulation of inhibitory connections by astrocytes (mediated in biology by different mechanisms) could be an interesting point for discussion and a future study if one tries to encode images by stimulus specific inhibition.

Finally, the use of astrocytic modulation of neuronal activity extends the standard capabilities of spiking neural networks due to the slow modulation of synaptic connections, which in turn can be considered a kind of “fine tuning” action “slowly” optimizing the weights along with the major algorithms’ change of synaptic connections. This potential can be used in the design of new learning techniques in spiking-neural-network-based information processing.

**Supplementary Materials:** The following supporting information can be downloaded at: <https://www.mdpi.com/article/10.3390/math11030561/s1>. References [39–41] are cited in Supplementary Materials.

**Author Contributions:** Conceptualization, S.V.S.; methodology, S.V.S.; software, S.V.S.; validation, S.V.S.; formal analysis, S.V.S.; investigation, S.V.S.; resources, S.V.S.; data curation, S.V.S.; writing—original draft preparation, S.V.S. and V.B.K.; writing—review and editing, S.V.S. and V.B.K.; visualization, S.V.S.; supervision, S.V.S.; project administration, S.V.S. and V.B.K.; funding acquisition, S.V.S. and V.B.K. All authors have read and agreed to the published version of the manuscript.

**Funding:** This research was funded by MIPT Priority 2030 Program.

**Institutional Review Board Statement:** Not applicable.

**Informed Consent Statement:** Not applicable.

**Data Availability Statement:** The data that support the findings of this study are available from the corresponding author upon reasonable request.

**Conflicts of Interest:** The authors declare no conflict of interest.

## Appendix A

### Appendix A.1. Cases with Numbers from Database MNIST

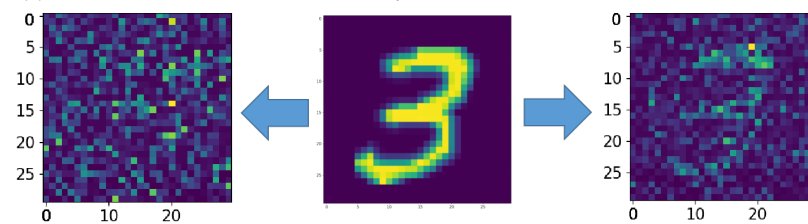


**Figure A1.** The middle picture is the supplied pattern (3 from handwritten database MNIST (MNIST dataset is made available under the terms of the Creative Commons Attribution-Share Alike 3.0 license)) [39], on the left, encoded by the spiking neural network without astrocyte modulation and noise amplitude  $A_{noise} = 6$ , and on the right, with astrocyte modulation and noise amplitude  $A_{noise} = 6$ .

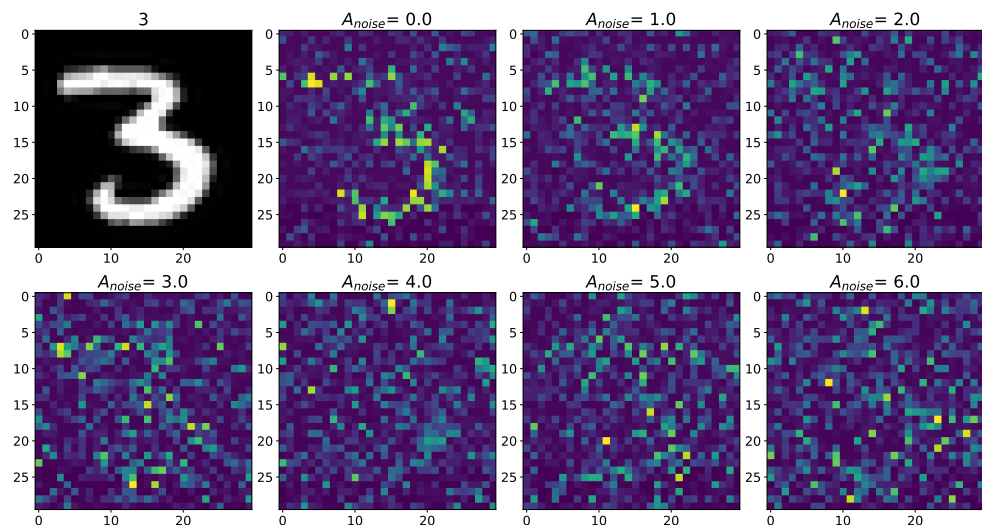


**Figure A2.** Changes in the spatial sweep of the spiking neural network during the representation of the supplied image from the Figure A1 when the amplitude,  $A_{noise}$ , of the noise current,  $I_{noise}$ , changes from 0 to 6 without modulation of neuronal activity by astrocytes.

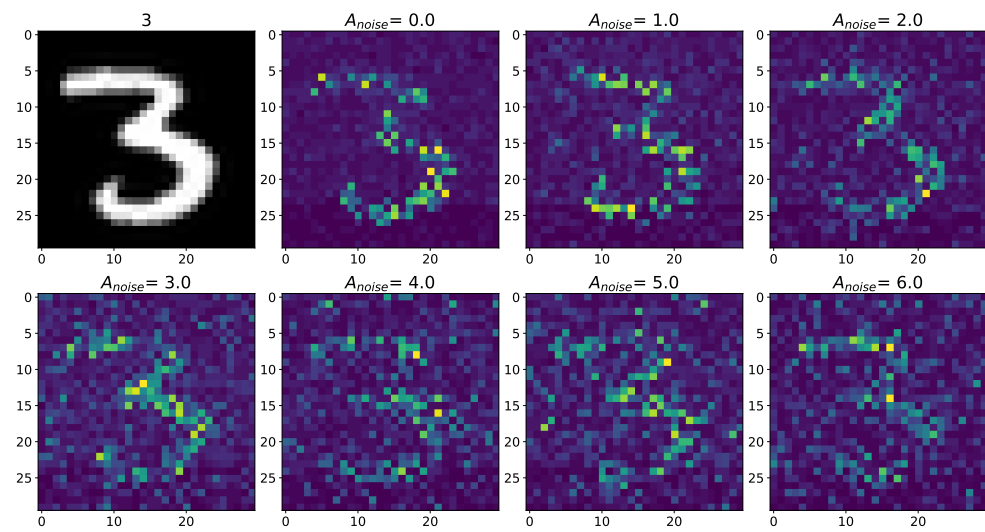


**Figure A3.** Changes in the spatial sweep of the spiking neural network during the representation of the supplied image from the Figure A1 when the amplitude,  $A_{noise}$ , of the noise current,  $I_{noise}$ , changes from 0 to 6 with modulation of neuronal activity by astrocytes.

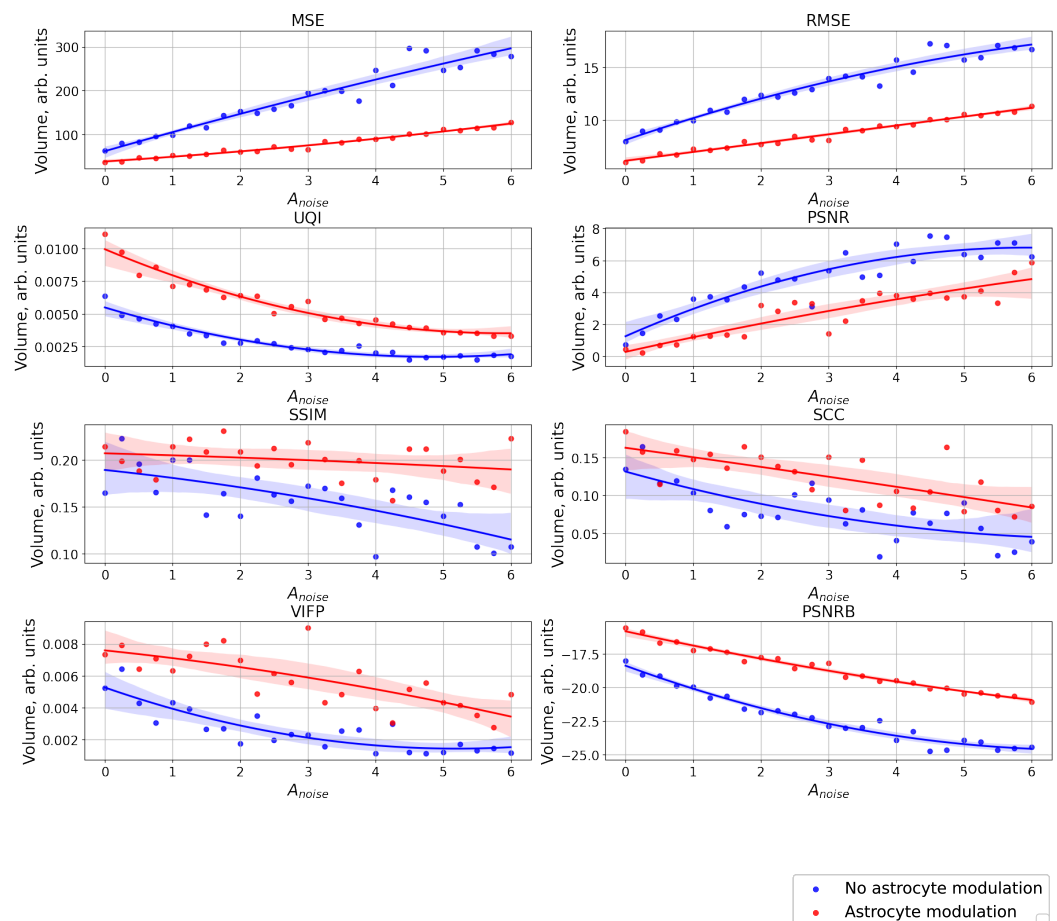


**Figure A4.** The case of using quality metrics—MSE, RMSE, UQI, PSNR, SSIM, SCC, VIFP, and PSNRB—for comparing raster diagrams of neural activity from Figures A2 and A3 with an image (middle panel of Figure A1) fed to a spiking neural network with an increase in the amplitude,  $A_{noise}$ , of the noise signal from 0 to 6 supplied to the neurons of the neural network without astrocytic modulation (blue dots and curve) and with astrocytic modulation (red dots and curve).



## Appendix A.2

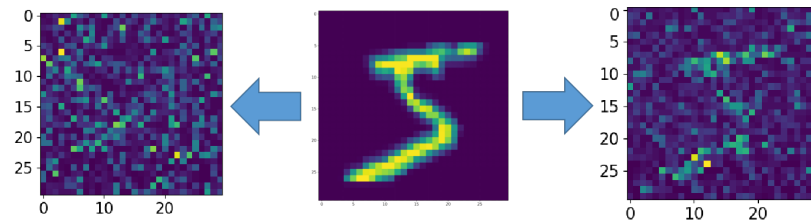


**Figure A5.** The middle picture is the supplied pattern (5 from handwritten database MNIST (MNIST dataset is made available under the terms of the Creative Commons Attribution-Share Alike 3.0 license)) [39], on the left, encoded by the spiking neural network without astrocyte modulation and noise amplitude  $A_{noise} = 6$ , and on the right, with astrocyte modulation and noise amplitude  $A_{noise} = 6$ .

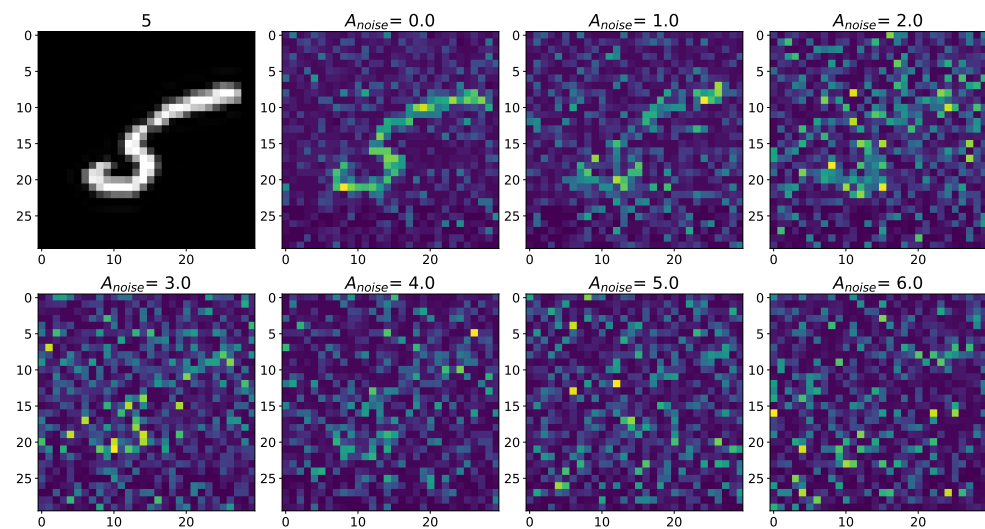


**Figure A6.** Changes in the spatial sweep of the spiking neural network during the representation of the supplied image from the Figure A5 when the amplitude,  $A_{noise}$ , of the noise current,  $I_{noise}$ , changes from 0 to 6 without modulation of neuronal activity by astrocytes.

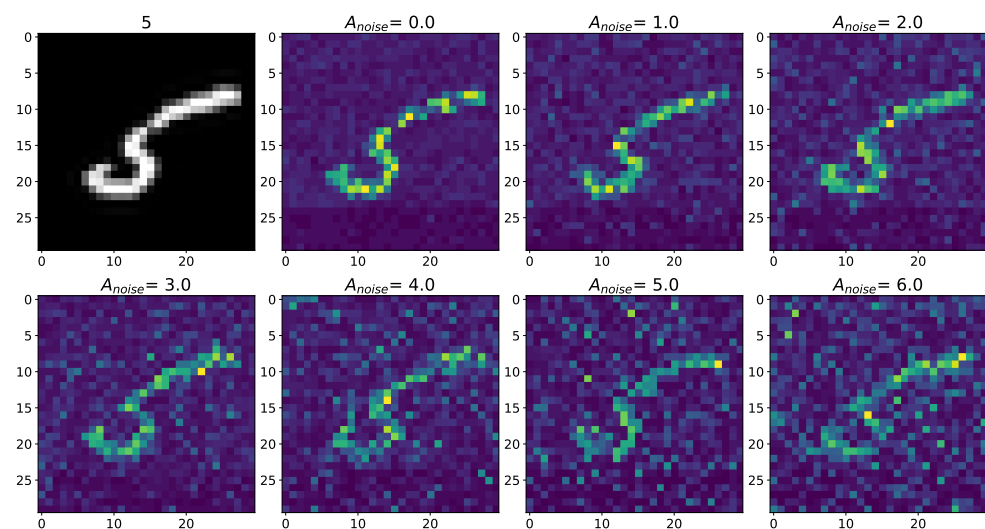


**Figure A7.** Changes in the spatial sweep of the spiking neural network during the representation of the supplied image from the Figure A5 when the amplitude,  $A_{noise}$ , of the noise current,  $I_{noise}$ , changes from 0 to 6 with modulation of neuronal activity by astrocytes.

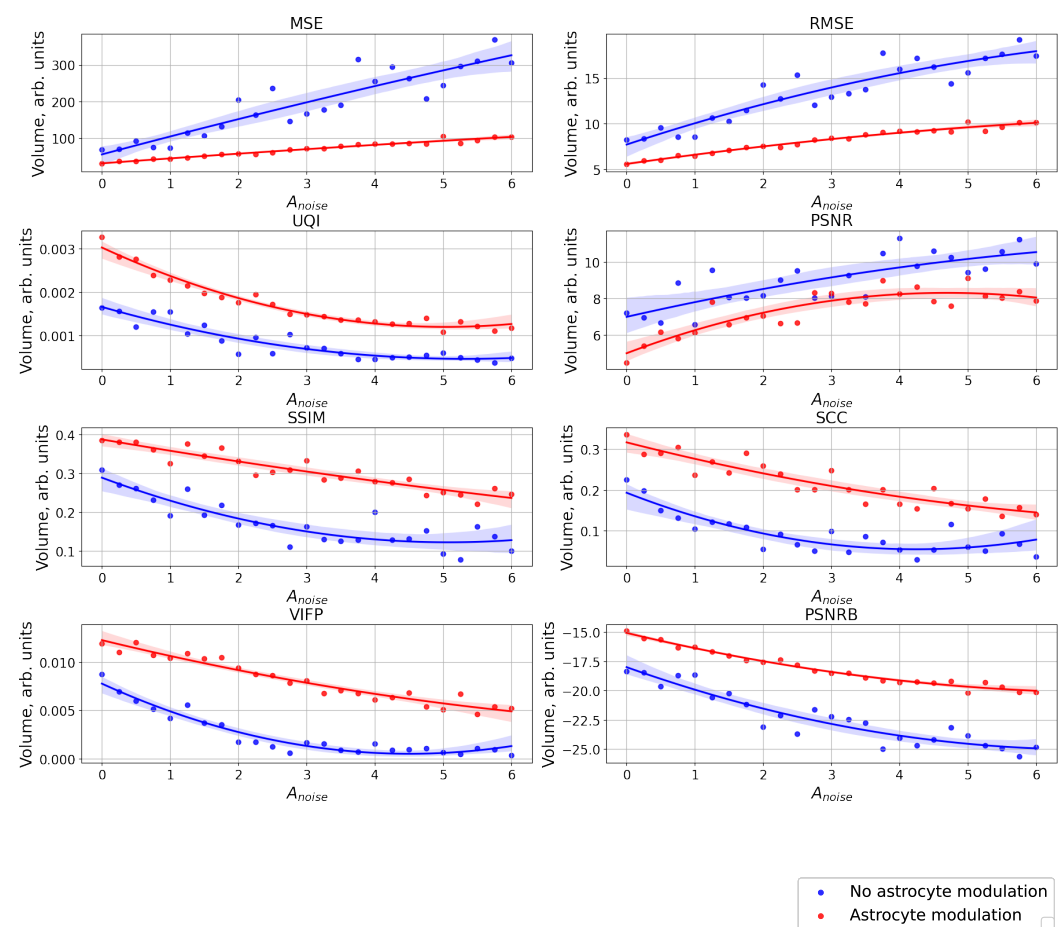


**Figure A8.** The case of using quality metrics—MSE, RMSE, UQI, PSNR, SSIM, SCC, VIFP, and PSNRB—for comparing raster diagrams of neural activity from Figures A6 and A7 with an image (middle panel of Figure A5) fed to a spiking neural network with an increase in the amplitude,  $A_{noise}$ , of the noise signal from 0 to 6 supplied to the neurons of the neural network without astrocytic modulation (blue dots and curve) and with astrocytic modulation (red dots and curve).

## References

1. Araque, A.; Parpura, V.; Sanzgiri, R.; Haydon, P. Glutamate-dependent astrocyte modulation of synaptic transmission between cultured hippocampal neurons. *Eur. J. Neurosci.* **1998**, *10*, 2129–2142.
2. Araque, A.; Parpura, V.; Sanzgiri, R.; Haydon, P. Tripartite synapses: Glia, the unacknowledged partner. *Trends Neurosci.* **1999**, *22*, 208–215.
3. Wittenberg, G.; Sullivan, M.; Tsien, J. Synaptic reentry reinforcement based network model for long-term memory consolidation. *Hippocampus* **2002**, *12*, 637–647.
4. Wang, X. Synaptic basis of cortical persistent activity: The importance of NMDA receptors to working memory. *J. Neurosci. Off. J. Soc. Neurosci.* **1999**, *19*, 9587–9603.
5. Haydon, P.G. GLIA: Listening and talking to the synapse. *Nat. Rev. Neurosci.* **2001**, *2*, 185–193.
6. Perea, G.; Navarrete, M.; Araque, A. Tripartite synapses: Astrocytes process and control synaptic information. *Trends Neurosci.* **2009**, *32*, 421–431.
7. Nadkarni, S.; Jung, P. Dressed neurons: Modeling neural-glia interactions. *Phys. Biol.* **2004**, *1*, 35–41.
8. Nadkarni, S.; Jung, P. Modeling synaptic transmission of the tripartite synapse. *Phys. Biol.* **2007**, *4*, 1–9.
9. Volman, V.; Ben-Jacob, E.; Levine, H. The astrocyte as a gatekeeper of synaptic information transfer. *Neural Comput.* **2007**, *326*, 303–326.
10. De Pitta, M.; Volman, V.; Berry, H.; Ben-Jacob, E. A tale of two stories: Astrocyte regulation of synaptic depression and facilitation. *PLoS Comput. Biol.* **2011**, *7*, e1002293.
11. Postnov, D.; Ryazanova, L.; Sosnovtseva, O. Functional modeling of neural-glia interaction. *Bio Syst.* **2007**, *89*, 84–91.
12. Amiri, M.; Bahrami, F.; Janahmadi, M. Functional contributions of astrocytes in synchronization of a neuronal network model. *J. Theor. Biol.* **2011**, *292C*, 60–70.

13. Wade, J.; McDaid, L.; Harkin, J.; Crunelli, V.; Kelso, J. Bidirectional Coupling between Astrocytes and Neurons Mediates Learning and Dynamic Coordination in the Brain: A Multiple Modeling Approach. *PLoS ONE* **2011**, *6*, e29445.
14. Amiri, M.; Hosseinmardi, N.; Bahrami, F.; Janahmadi, M. Astrocyte-neuron interaction as a mechanism responsible for generation of neural synchrony: A study based on modeling and experiments. *J. Comput. Neurosci.* **2013**, *34*, 489–504.
15. Pankratova, E.; Kalyakulina, A.; Stasenko, S.; Gordleeva, S.; Lazarevich, I.; Kazantsev, V. Neuronal synchronization enhanced by neuron–astrocyte interaction. *Nonlinear Dyn.* **2019**, *97*, 647–662.
16. Ullah, G.; Jung, P.; Cornell-Bell, A. Anti-phase calcium oscillations in astrocytes via inositol (1, 4, 5)-trisphosphate regeneration. *Cell Calcium* **2006**, *39*, 197–208.
17. Kazantsev, V. Spontaneous calcium signals induced by gap junctions in a network model of astrocytes. *Phys. Rev. E Stat. Nonlinear Soft Matter Phys.* **2009**, *79*, 010901.
18. Verisokin, A.; Vervevko, D.; Postnov, D.; Brazhe, A. Modeling of astrocyte networks: Toward realistic topology and dynamics. *Front. Cell. Neurosci.* **2021**, *15*, 645068.
19. Wallach, G.; Lallouette, J.; Herzog, N.; De Pitta, M.; Jacob, E.; Berry, H.; Hanein, Y. Glutamate mediated astrocytic filtering of neuronal activity. *PLoS Comput. Biol.* **2014**, *10*, e1003964.
20. Riera, J.; Hatanaka, R.; Ozaki, T.; Kawashima, R. Modeling the spontaneous  $\text{Ca}^{2+}$  oscillations in astrocytes: Inconsistencies and usefulness. *J. Integr. Neurosci.* **2011**, *10*, 439–473.
21. Manninen, T.; Havela, R.; Linne, M. Computational models for calcium-mediated astrocyte functions. *Front. Comput. Neurosci.* **2018**, *12*, 14.
22. Gordleeva, S.; Tsybina, Y.; Krivonosov, M.; Ivanchenko, M.; Zaikin, A.; Kazantsev, V.; Gorban, A. Modeling working memory in a spiking neuron network accompanied by astrocytes. *Front. Cell. Neurosci.* **2021**, *15*, 631485.
23. Tsybina, Y.; Kastalskiy, I.; Krivonosov, M.; Zaikin, A.; Kazantsev, V.; Gorban, A.; Gordleeva, S. Astrocytes mediate analogous memory in a multi-layer neuron–astrocyte network. *Neural Comput. Appl.* **2022**, *34*, 9147–9160.
24. Gordleeva, S.; Tsybina, Y.; Krivonosov, M.; Tyukin, I.; Kazantsev, V.; Zaikin, A.; Gorban, A. Situation-based memory in spiking neuron-astrocyte network. *arXiv* **2022**, arXiv:2202.07218.
25. Hodgkin, A.; Huxley, A. A quantitative description of membrane current and its application to conduction and excitation in nerve. *J. Physiol.* **1952**, *117*, 500–544.
26. Izhikevich, E.M. *Dynamical Systems in Neuroscience: The Geometry of Excitability and Bursting*, 1st ed.; The MIT Press: Cambridge, MA, USA, 2007; p. 441.
27. Angulo, M.; Kozlov, A.; Charpak, S.; Audinat, E. Glutamate released from glial cells synchronizes neuronal activity in the hippocampus. *J. Neurosci.* **2004**, *24*, 6920–6927. <https://doi.org/10.1523/JNEUROSCI.0473-04.2004>.
28. Halassa, M.; Fellin, T.; Haydon, P. Tripartite synapses: Roles for astrocytic purines in the control of synaptic physiology and behavior. *Neuropharmacology* **2009**, *57*, 343–346.
29. Gordleeva, S.; Stasenko, S.; Semyanov, A.; Dityatev, A.; Kazantsev, V. Bi-directional astrocytic regulation of neuronal activity within a network. *Front. Comput. Neurosci.* **2012**, *6*, 92.
30. Lazarevich, I.; Stasenko, S.; Kazantsev, V. Synaptic multistability and network synchronization induced by the neuron–glial interaction in the brain. *JETP Lett.* **2017**, *105*, 210–213.
31. Stasenko, S.; Lazarevich, I.; Kazantsev, V. Quasi-synchronous neuronal activity of the network induced by astrocytes. *Procedia Comput. Sci.* **2020**, *169*, 704–709.
32. Martín, E.; Fernández, M.; Perea, G.; Pascual, O.; Haydon, P.; Araque, A.; Ceña, V. Adenosine released by astrocytes contributes to hypoxia-induced modulation of synaptic transmission. *Glia* **2007**, *55*, 36–45.
33. Jourdain, P.; Bergersen, L.; Bhaukaurally, K.; Bezzi, P.; Santello, M.; Domercq, M.; Matute, C.; Tonello, F.; Gundersen, V.; Volterra, A. Glutamate exocytosis from astrocytes controls synaptic strength. *Nat. Neurosci.* **2007**, *10*, 331–339.
34. Fiocco, T.; McCarthy, K. Intracellular astrocyte calcium waves in situ increase the frequency of spontaneous AMPA receptor currents in CA1 pyramidal neurons. *J. Neurosci.* **2004**, *24*, 722–732.
35. Rusakov, D.; Kullmann, D. Extrasynaptic glutamate diffusion in the hippocampus: Ultrastructural constraints, uptake, and receptor activation. *J. Neurosci.* **1998**, *18*, 3158–3170.
36. Van Rossum, G.; Drake, F., Jr. *Python Tutorial*; Centrum voor Wiskunde en Informatica Amsterdam: Amsterdam, The Netherlands, 1995.
37. Stimberg, M.; Brette, R.; Goodman, D. Brian 2, an intuitive and efficient neural simulator. *Elife* **2019**, *8*, e47314.
38. Hunter, J. Matplotlib: A 2D graphics environment. *Comput. Sci. Eng.* **2007**, *9*, 90–95.
39. LeCun, Y.; Cortes, C.; Burges, C. MNIST Handwritten Digit Database. 2010. Available online: <http://yann.lecun.com/exdb/mnist> (accessed on 1 November 2022).
40. Xiao, H.; Rasul, K.; Vollgraf, R. Fashion-mnist: a novel image dataset for benchmarking machine learning algorithms. *arXiv* **2017**, arXiv:1708.07747.
41. Yang, R.; Deng, Y.; Zhu, A.; Tong, X.; Chen, Z. Few Shot Learning Based on the Street View House Numbers (SVHN) Dataset. In *International Conference on Edge Computing and IoT*; Springer: Cham, Switzerland, 2021; pp. 86–102.
42. Sara, U.; Akter, M.; Uddin, M. Image quality assessment through FSIM, SSIM, MSE and PSNR—A comparative study. *J. Comput. Commun.* **2019**, *7*, 8–18.
43. Wang, Z.; Bovik, A. A universal image quality index. *IEEE Signal Process. Lett.* **2002**, *9*, 81–84.

44. Manninen, T.; Saudargienė, A.; Linne, M. Astrocytic modulation of cortical synaptic plasticity: Integrating biological knowledge and computational modeling. In *Glia: XV European Meeting on Glial Cells in Health and Disease Online-GLIA: Abstract Book: 5–9 July 2021*; Wiley-Liss: New York, NY, USA, 2021; Volume 69, pp. E335–E4335.
45. Wang, Y.; Fu, A.; Ip, N. Instructive roles of astrocytes in hippocampal synaptic plasticity: Neuronal activity-dependent regulatory mechanisms. *Febs J.* **2022**, *289*, 2202–2218.
46. Noriega-Prieto, J.; Araque, A. Sensing and regulating synaptic activity by astrocytes at tripartite synapse. *Neurochem. Res.* **2021**, *46*, 2580–2585.
47. González-Arias, C.; Perea, G. Gliotransmission at tripartite synapses. In *Computational Glioscience*; Springer: Cham, Switzerland, 2019; pp. 213–226.
48. Santello, M.; Toni, N.; Volterra, A. Astrocyte function from information processing to cognition and cognitive impairment. *Nat. Neurosci.* **2019**, *22*, 154–166.
49. Kol, A.; Adamsky, A.; Groysman, M.; Kreisel, T.; London, M.; Goshen, I. Astrocytes contribute to remote memory formation by modulating hippocampal–cortical communication during learning. *Nat. Neurosci.* **2020**, *23*, 1229–1239.
50. Kastanenka, K.; Moreno-Bote, R.; De Pittà, M.; Perea, G.; Eraso-Pichot, A.; Masgrau, R.; Poskanzer, K.; Galea, E. A roadmap to integrate astrocytes into Systems Neuroscience. *Glia* **2020**, *68*, 5–26.
51. Oliveira, J.; Araque, A. Astrocyte regulation of neural circuit activity and network states. *Glia* **2022**, *70*, 1455–1466.

**Disclaimer/Publisher’s Note:** The statements, opinions and data contained in all publications are solely those of the individual author(s) and contributor(s) and not of MDPI and/or the editor(s). MDPI and/or the editor(s) disclaim responsibility for any injury to people or property resulting from any ideas, methods, instructions or products referred to in the content.